

Effects of composite rheology on plate-like behavior in global-scale mantle convection

Maëlis Arnould^{1,2}, Tobias Rolf^{2,3} and Antonio Manjón-Cabeza Córdoba^{2,4,5}

¹University of Lyon, UCBL, ENSL, UJM, CNRS 5276, Laboratoire de Géologie de Lyon - Terre, Planètes,
Environnement, Lyon, France

²Centre for Earth Evolution and Dynamics, Department of Geosciences, University of Oslo, Blindern,
Oslo, Norway

³Institute of Geophysics, University of Münster, Germany

⁴Andalusian Earth Sciences Institute, University of Granada, Spain

⁵Department of Earth Sciences, University College London, UK

Key Points:

- Uppermost mantle viscosity variations induced by composite rheology control surface tectonics
- Composite rheology can impede or enhance plate mobility depending on lithospheric strength
- Composite rheology does not facilitate the onset of subduction for large yield stress

Corresponding author: Maelis Arnould, maelis.arnould@univ-lyon1.fr

Abstract

Earth's upper mantle rheology controls lithosphere-asthenosphere coupling and thus surface tectonics. Rock deformation experiments and seismic anisotropy measurements indicate that composite rheology (co-existing diffusion and dislocation creep) occurs in the Earth's uppermost mantle, potentially affecting convection and surface tectonics. Here, we investigate how the spatio-temporal distribution of dislocation creep in an otherwise diffusion-creep-controlled mantle impacts the planform of convection and the planetary tectonic regime as a function of the lithospheric yield strength in numerical models of mantle convection self-generating plate-like tectonics. The low upper-mantle viscosities caused by zones of substantial dislocation creep produce contrasting effects on surface dynamics. For strong lithosphere (yield strength >35 MPa), the large lithosphere-asthenosphere viscosity contrasts promote stagnant-lid convection. In contrast, the increase of upper mantle convective vigor enhances plate mobility for lithospheric strength <35 MPa. For the here-used model assumptions, composite rheology does not facilitate the onset of plate-like behavior at large lithospheric strength.

Plain Language Summary

Understanding uppermost mantle flow and deformation is important to study Earth's surface evolution, since plate tectonics and mantle convection are intertwined processes. Observations and experiments provide important - yet uncertain - constraints suggesting that uppermost mantle viscosity should be at least partially controlled by dislocation creep (i.e. its rheology should vary non-linearly with stress). However, most studies have not included dislocation creep. Here, we incorporate different amounts of this deformation mechanism in global-scale numerical models of mantle convection featuring Earth-like tectonic plates. We demonstrate that fast-evolving low-viscosity areas containing dislocation creep arise around slabs and plumes. Moreover, large amounts of dislocation creep alter surface tectonics in several ways: for a weak lithosphere, subductions become shorter-lived and plate velocities increase. For a strong lithosphere, in contrast, plate tectonics is inhibited. This study therefore demonstrates the key role of composite rheology in understanding mantle-lithosphere interactions.

1 Introduction

The lithospheric behavior of terrestrial bodies notably depends on their mantle properties and dynamics (e.g. Alisic et al., 2012; Coltice et al., 2017; Garel et al., 2020). In particular, mantle rheology determines the coupling between the convecting mantle and the lithosphere, therefore affecting surface heat transfer, plate velocities and continental motions (e.g. Stein et al., 2004; Rolf et al., 2018). Rock-deformation laboratory experiments conducted at upper-mantle conditions (Fig 1a-b, e.g. Hirth & Kohlstedt, 2003; Karato & Wu, 1993) show that mantle rheology is composite, meaning that deformation is driven by a coexistence of different creep mechanisms such as diffusion creep (linear or Newtonian stress/strain-rate dependence) and dislocation creep (non-linear power-law or non-Newtonian stress/strain-rate relationship). These experimental results are corroborated by the observed spatial heterogeneity in the strength of uppermost-mantle seismic anisotropy (e.g. Beghein et al., 2014; Debayle & Ricard, 2013), which could be at least partially explained by different amounts of olivine lattice preferred orientations (LPO), possibly caused by the heterogeneous development of dislocation creep in the uppermost mantle (e.g. Becker et al., 2006; Hedjazian et al., 2017; Nicolas & Christensen, 1987).

While mantle composite rheology is typically considered in regional-scale geodynamics models (e.g. Billen & Hirth, 2005; Garel et al., 2020; Neuharth & Mittelstaedt, 2023), it is often neglected in global-scale models (e.g. Coltice et al., 2017; Li & Zhong, 2019; Stein et al., 2004), or simply mimicked by reduced activation energy in pure diffusion creep rheology (Christensen, 1983, 1984). However, this latter approximation causes differences in the planform of stagnant-lid convection compared to using full composite rheology (e.g. Schulz et al., 2020). Moreover, prescribing pure diffusion creep makes it difficult to fully capture Earth's lithosphere and mantle behavior, such as observed plume swells' shapes (Asaadi et al., 2011), trench retreat rates (Holt & Becker, 2016), seismic anisotropy patterns around slabs (Jadamec & Billen, 2010), surface dynamic topography amplitudes (e.g. Bodur & Rey, 2019), and subduction geometry during its initiation (e.g. Billen & Hirth, 2005). Numerical studies prescribing pure dislocation creep in the upper-mantle have shown its importance for all these processes. However, in a composite formulation, the spatiotemporal distribution of the different creep mechanisms is not determined a priori, but arises self-consistently. Accounting for it therefore allows us to evaluate where substantial dislocation creep may occur in the mantle and to fur-

79 ther study its effects on geodynamic processes. Some global models of mantle convec-
 80 tion with plate-like behavior recently included composite rheology (e.g. Dannberg et al.,
 81 2017; Rozel, 2012), but these computationally-demanding models used a single set of rhe-
 82 ological activation parameters based on experimental values, while estimates vary over
 83 a large range (e.g. Ranalli, 2001; Korenaga & Karato, 2008; Jain et al., 2018, 2019). More-
 84 over, these numerical studies focussed on the effect of grain-size evolution on the plan-
 85 form of convection and on the lithospheric behavior. Therefore, a systematic exploration
 86 of the effects of composite rheology in the upper mantle is still needed.

87 Here, we explore how the temperature-, depth- and stress-dependent diffusion/dislocation
 88 creep partitioning impacts the planform of convection and the tectonic regime in 2D-cartesian
 89 whole-mantle convection models with composite rheology and static grain-size self-generating
 90 plate tectonics. Our goal is not to use Earth-like rheological parameters, but rather in-
 91 vestigate the geodynamic effects of different parametrizations of composite rheology and
 92 capture qualitative convective and tectonic trends relevant for the Earth (Fig. 1). We
 93 find that composite rheology influences both mantle convective planform and surface tec-
 94 tonics due to its spatio-temporal dynamic effect on uppermost mantle viscosity, either
 95 enhancing or altering plate mobility and plateness depending on lithospheric strength.
 96 These results demonstrate that uncertainties in experimentally-determined rheological
 97 parameters lead to substantial geodynamical effects, and calls for further consideration
 98 of composite rheology in studies of mantle-lithosphere interactions.

99 2 Methods

100 2.1 On the use of composite rheology

101 Mantle viscosity varies with temperature (T), pressure (P), grain-size (d) and stress
 102 (σ) (e.g. Hirth & Kohlstedt, 2003; Karato & Wu, 1993):

$$\eta_{mech} = A_{mech} d^m \sigma^{1-n} \exp\left(\frac{E_{mech} + PV_{mech}}{RT}\right). \quad (1)$$

103 R is the gas constant, m is the grain-size exponent and n is the stress exponent. E_{mech} ,
 104 V_{mech} and A_{mech} are respectively the activation energy, the activation volume and a pre-
 105 exponential factor (accounting for all other effects on mantle rheology, such as water and
 106 melt content) for the rheological mechanism ($mech$) considered (diffusion or dislocation
 107 creep).

108 Diffusion creep dominates below and dislocation creep dominates above the tran-
 109 sition stress (σ_t) at which the strain-rates due to the two different mechanisms are equal
 110 ($\dot{\epsilon}_{diff} = \dot{\epsilon}_{disl}$, e.g. Christensen, 1984; Hall & Parmentier, 2003):

$$\sigma_t = \left(\frac{A_{diff}}{A_{disl}} \right)^{\frac{1}{n-1}} d^{-\frac{m}{n-1}} \exp \left(\frac{(E_{disl} - E_{diff}) + P(V_{disl} - V_{diff})}{RT} \right)^{\frac{1}{n-1}}. \quad (2)$$

111 E_{diff} , E_{disl} , V_{diff} and V_{disl} can be determined for olivine from rock experiments (e.g.
 112 Karato & Wu, 1993) and vary respectively between 240–450 kJ/mol, 430–560 kJ/mol,
 113 0 – 20 cm³/mol and 0 – 33 cm³/mol (Hirth & Kohlstedt, 2003; Karato & Wu, 1993;
 114 Ranalli, 2001), depending on water content. Despite those uncertainties, $E_{diff} < E_{disl}$
 115 and $V_{diff} < V_{disl}$ (Fig. 1a-b, e.g Karato & Wu, 1993). Those experiments predict that
 116 dislocation creep should dominate in hot regions of the uppermost-mantle and areas sub-
 117 mitted to high stresses (Fig. 1a-b).

118 2.2 Numerical model setup

119 We solve the non-dimensional equations of mass, momentum and energy conser-
 120 vation under the Boussinesq approximation using StagYY (e.g. Tackley, 2000a) on a 2D-
 121 cartesian 512x128 or 768x192 grid (aspect ratio 4:1). Grid cells are refined near the ther-
 122 mal boundary layers. Top and bottom boundaries are free-slip, lateral boundaries are
 123 periodic. We use a reference Rayleigh number of 10^7 . The mantle is heated both from
 124 below and from within (constant internal heating rate $H = 8.6 \times 10^{-12}$ W kg⁻¹, Ta-
 125 ble S1).

126 We use a pseudoplastic rheology to model plate-like behavior (e.g. Trompert & Hansen,
 127 1998; Tackley, 2000a), and vary the surface yield stress σ_{Y0} , which represents lithospheric
 128 strength, between 12 and 234 MPa. The yield stress varies with depth at a rate of ~ 0.3
 129 MPa km⁻¹. The surface yield stress is bounded by the typical stress drop during earth-
 130 quakes (10 MPa, Allmann & Shearer, 2009) and the yield stress of pristine lithospheric
 131 rocks measured in experiments (Brace & Kohlstedt, 1980). Over the modeled range of
 132 yield stresses, diverse tectonic behaviors are expected for pure diffusion creep: from mo-
 133 bile plates at low yield stress to stagnant-lid at high yield stress (e.g. Arnould et al., 2018).

134 In StagYY, the transition stress σ_t^* between diffusion and dislocation creep is de-
 135 fined in analogy to Eq. 2 as:

$$\sigma_t^* = \sigma_0 \left(\frac{B_{disl}}{B_{diff}} \right)^{\frac{1}{n-1}} \left(\frac{d}{d_0} \right)^{-\frac{m}{n-1}} \exp \left(\frac{(E_{disl} - E_{diff}) + P(V_{disl} - V_{diff})}{R(T + T_0 - T_{surf})} \right)^{\frac{1}{n-1}}. \quad (3)$$

136 $T_0 = 0.64$ is the non-dimensional reference temperature, equivalent to 1,600 K and $T_{surf} =$
 137 0.12 is the non-dimensional surface temperature, equivalent to 300 K. σ_0 is a reference
 138 transition stress. B_{diff} and B_{disl} differ from A_{mech} in Eq. 1 and ensure that mantle vis-
 139 cosity equals the non-dimensional reference viscosity $\eta_0 = 1$ (9.8×10^{21} Pa s) at refer-
 140 ence conditions (temperature of 1,600 K and surface pressure). As we do not account
 141 for grain-size evolution, $d = d_0$ unless explicitly mentioned otherwise (see Discussion
 142 in section 4). For dislocation creep, $m=0$ and $n=3.5$ while for diffusion creep, $m=2$ and
 143 $n=1$.

144 **2.3 Computed cases**

145 For each value of σ_{Y_0} , we fix E_{diff} , V_{diff} , and E_{disl} , but vary V_{disl} by a factor of
 146 ~ 3 , since its experimental value is subjected to the largest uncertainties (e.g. Karato &
 147 Wu, 1993; Korenaga & Karato, 2008). We also vary σ_0 between 1.2 and 3.5 MPa to en-
 148 sure that dislocation creep is mostly restricted to the upper mantle. We choose lower ac-
 149 tivation parameters than experimentally determined for pristine olivine for reasons of
 150 numerical feasibility. Instead, we preserve ranges of variation for $E_{disl} - E_{diff}$ and $V_{disl} -$
 151 V_{diff} similar to rock experiments (Karato and Wu (1993), Fig. 1) since these differences
 152 matter the most in Eq. 2 and 3. The spatio-temporal evolution of mantle convection self-
 153 consistently partitions the mantle into areas dominated by dislocation creep or diffusion
 154 creep, depending on the value of stress.

155 For each yield stress, we first ran models in pure diffusion creep over 3 Gyr, start-
 156 ing from a stratified thermal field with small perturbations to initiate convection. We
 157 then restarted from the final thermal field of these models while including composite rhe-
 158 ology and ran those new models over 3 Gyr. Since we do not model evolutionary mod-
 159 els, this procedure ensures that the models are in quasi-statistical steady-state (Fig. S2)
 160 during the last 400 Myr of each simulation that we analyse. Detailed model parameters,
 161 with their non-dimensional and dimensional values are given in Table S1.

162 **3 Results**

163 **3.1 Spatio-temporal distribution of dislocation creep**

164 Decreasing both V_{disl} and/or σ_0 results in a thicker and more continuous layer de-
 165 forming in dislocation creep in the upper mantle (Fig. 2). As a consequence, upper man-

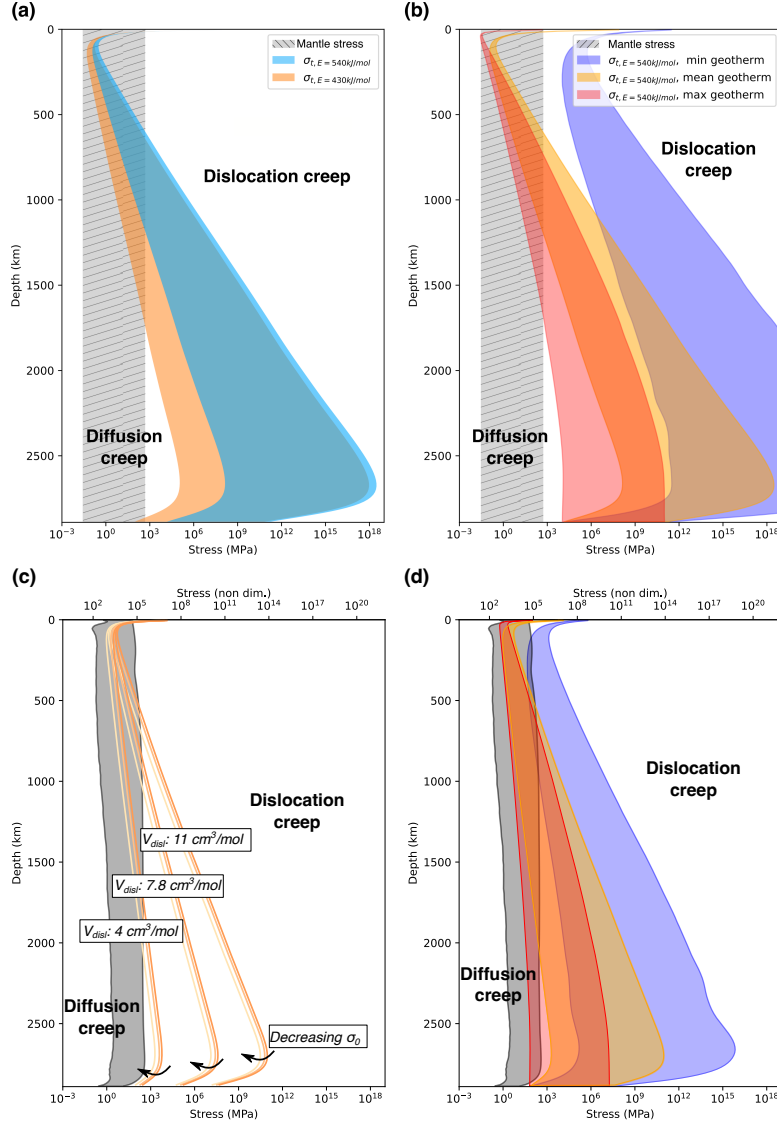


Figure 1. **Top:** Range of olivine transition stress measured by Karato and Wu (1993), assuming a grain-size of 1 mm. (a) Sensitivity to E_{disl} (blue: 430 kJ mol⁻¹, orange: 540 kJ mol⁻¹) and V_{disl} (10-25 cm³ mol⁻¹), using an average geotherm from a reference model in pure diffusion creep (Fig. S1e). (b) Sensitivity to temperature using $E_{disl} = 430$ kJ mol⁻¹ and $10 < V_{disl} < 25$ cm³ mol⁻¹ (blue=cold, yellow=average, and red=hot geotherm (Fig. S1e)). **Bottom:** Same as above, but for our modeling setup. (c) Sensitivity of the model transition stress to V_{disl} (4-11 cm³ mol⁻¹) and σ_0 (1.2-3.5 MPa), using an average geotherm (Fig. S1e). (d) Sensitivity to temperature. In all panels, gray-striped areas show the stress range expected in Earth’s mantle (top) and predicted in our reference model (bottom, Fig. S1b).

166 the viscosity decreases by at least one order of magnitude on average. Moreover, aver-
 167 age horizontal and vertical velocities increase by a factor of 3 depending on the amount
 168 of dislocation creep (Fig. 2a), irrespective of the surface yield stress (Fig. S3), showing
 169 that composite rheology enhances convective vigor locally. Due to its location and low
 170 viscosity signature, the layer containing $>10\%$ dislocation creep is here-after referred to
 171 as an “asthenosphere” in models with composite rheology, although it sometimes locally
 172 reaches lower-mantle depths (low V_{disl} and σ_0).

173 Areas strongly affected by dislocation creep show a high spatio-temporal variabil-
 174 ity within the asthenospheric layer (Fig. 2b-d and Supplementary Movie 1), which pro-
 175 duces large lateral viscosity variations in the upper mantle, as shown by e.g. Alisic et
 176 al. (2012); Billen and Hirth (2007); Semple and Lenardic (2020). In models featuring plate-
 177 like behavior, dislocation creep mainly occurs around slabs and plumes in the uppermost
 178 mantle. Indeed, ambient mantle shearing by sinking slabs is responsible for the highest
 179 convective stresses, and thus for a higher proportion of dislocation creep around them.
 180 In contrast and depending on their thickness, slab interiors deform mostly through dif-
 181 fusion creep (Fig. 2b-c) because of their much colder state (Fig. 1b and d). The evolu-
 182 tion of individual slabs is significantly affected by composite rheology, consistent with
 183 regional thermo-mechanical models (e.g. Garel et al., 2020): slabs tend to sink faster through
 184 an upper mantle with more abundant dislocation creep and thus a more pronounced low
 185 viscosity zone (Fig. 2). Moreover, they tend to buckle and/or break-off more easily de-
 186 pending on their strength and the mantle viscosity structure (Fig. 4a and d). In fact,
 187 both the amount of dislocation creep around slabs and the thickness of the asthenosphere
 188 are responsible for creating a viscosity contrast between the upper and the lower man-
 189 tle, which hinders the sinking of slabs and affects their evolution (Fig. 2a, e.g. Billen and
 190 Hirth (2007)).

191 Around plumes, hot mantle more likely deforms through dislocation creep (Fig. 1b
 192 and d), although shearing is less important than around slabs. Plumes are thus also sur-
 193 rounded by lower viscosities than pure diffusion creep cases, which favors fast rising (Fig.
 194 2 and Fig. S4). Plume material further tends to feed fast lateral asthenospheric channeled-
 195 flow (as proposed by e.g. Phipps Morgan et al., 1995) in which dislocation creep occurs
 196 more likely due to high temperatures and stresses, favoring even lower viscosity in these
 197 areas than in diffusion creep models (Fig. 2a and b). This occurs preferentially when new
 198 plume heads reach sub-lithospheric depths. Over a few million to a few tens of million

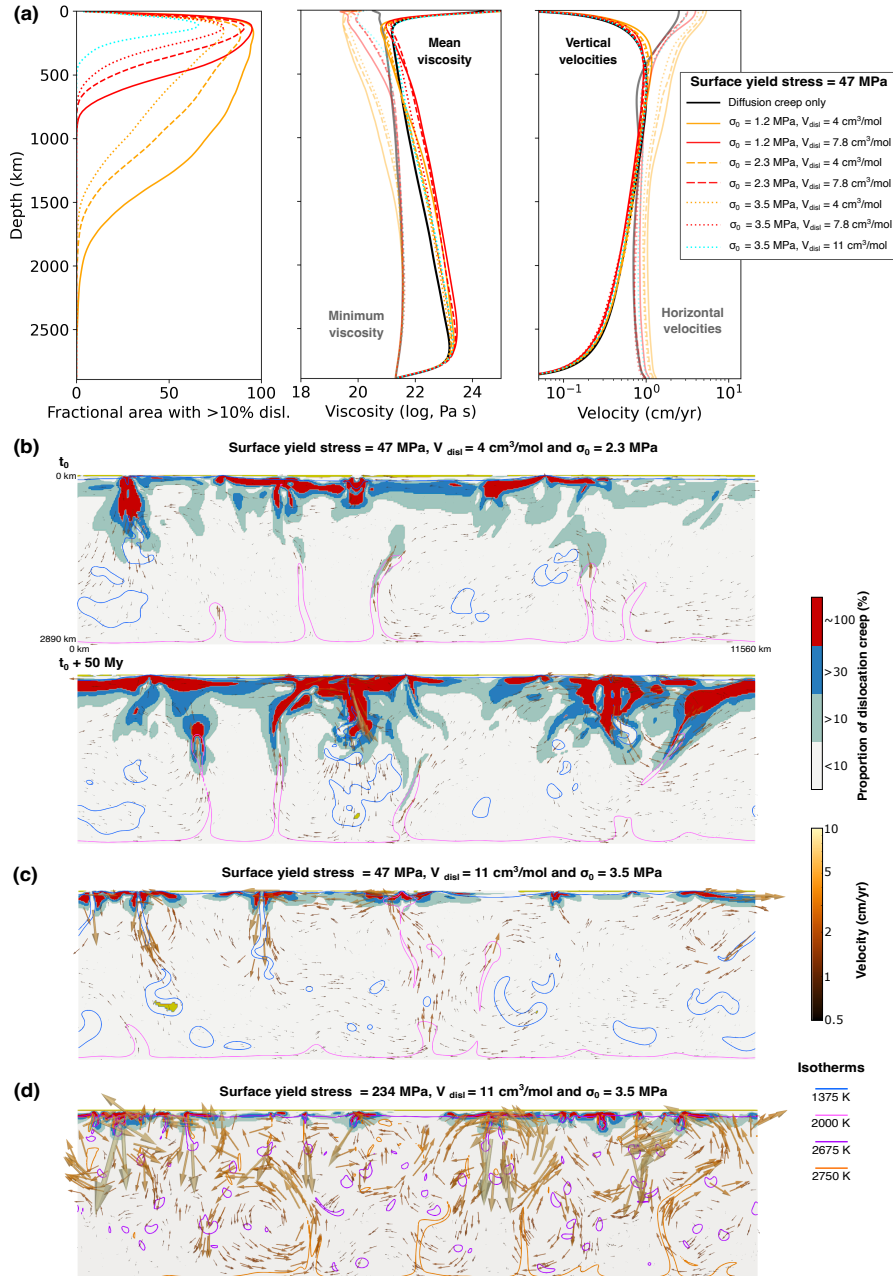


Figure 2. (a) Time-averaged profiles of (left) mantle fractional area with >10% dislocation creep, (middle) minimum and mean viscosity, and (right) vertical and horizontal velocity for models with a surface yield stress $\sigma_{Y0} = 47$ MPa. (b-d) Proportion of dislocation creep and mantle velocity field (arrows scaled and coloured by magnitude) in three models. In (b), a 50 Myr-evolution is shown. In (b-c), blue lines show slabs and magenta lines contour plumes. In (d), purple lines contour dripping lithosphere and orange lines show hotter-than-average upwellings.

199 years, the geometry and abundance of dislocation creep can therefore vary considerably
 200 (Fig. 2b and c), controlled by the dynamics of convective thermal heterogeneities.

201 Models with surface yield strength larger than 120 MPa experience stagnant-lid
 202 convection. In these models, the mantle is much warmer due to limited heat loss, thus
 203 favoring more vigorous and smaller-scale convection than in cases with plate-like behav-
 204 ior (Fig. 2). Higher temperature and increased convective vigor promote dislocation creep,
 205 which emerges in areas of basal lithosphere dripping, or around hotter-than-average up-
 206 wellings in the shallow mantle (Fig. 2c). The large variability of these processes controls
 207 the spatio-temporal distribution of dislocation creep.

208 **3.2 Effects on the tectonic regime**

209 The effect of composite rheology on the surface tectonic regime is quantified through
 210 surface mobility $M = \frac{v_{surf}}{v_{rms}}$ (with v_{surf} the average surface velocity and v_{rms} the vol-
 211 ume root-mean-square velocity) and plateness $P = 1 - \frac{def_{90}}{def_{90,iso}}$ (with def_{90} being the
 212 fractional surface area containing 90% of deformation, and $def_{90,iso}$ being the value for
 213 an isoviscous model, Tackley, 2000a). These proxies are close to 1 for the mobile-lid regime
 214 and tend to 0 in the stagnant-lid regime, with episodic transitioning between these end-
 215 members. In addition, we track the number of active subduction zones, detected from
 216 surface downward velocity peaks, and the lithospheric thickness, defined from the inflec-
 217 tion point of the time-averaged temperature profile (Fig. 3 and Fig. S5).

218 Regardless of the surface yield strength, lithosphere thickness decreases as the pro-
 219 portion of dislocation creep increases (Fig. 3a and Fig. S5), by up to 60% compared to
 220 diffusion creep models. In the asthenospheric areas strongly affected by dislocation creep,
 221 increased convective vigor tends to impede lithospheric growth due to more efficient con-
 222 vective erosion. Therefore, the thicker the layer with substantial dislocation creep, the
 223 thinner is the lithosphere for a given surface yield stress compared to pure diffusion-creep
 224 models. Besides the major control of surface lithospheric yield strength, composite rhe-
 225 ology has two contrasting effects on the tectonic regime. These effects are summarized
 226 on Fig. 4a-c and described below.

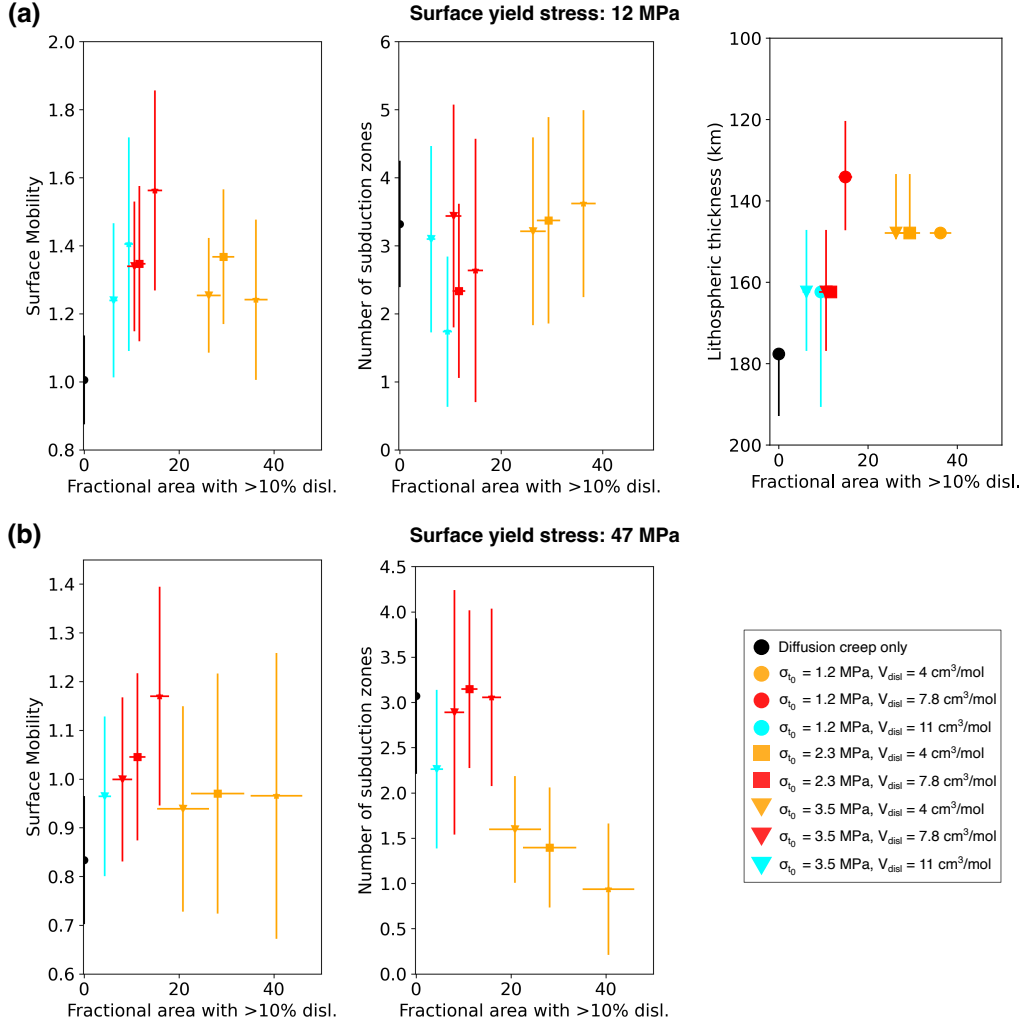


Figure 3. Effect of composite rheology on surface tectonic regime (temporal average and standard deviation of surface mobility, number of subduction zones and lithosphere thickness as a function of the time-averaged mantle fractional area containing >10% dislocation creep) in models with $\sigma_{Y_0} = 12$ MPa (a) and 47 MPa (b).

227

3.2.1 Models with a weak lithosphere (<35 MPa)

228

229

230

231

232

233

For yield stresses below ~ 35 MPa, models in pure diffusion creep are in the mobile-lid regime. Composite rheology enhances surface mobility (up to 1.6) and plateness. Active subduction zones tend to be shorter-lived (Fig. 4d). In these models, the viscosity reduction in the uppermost mantle induced by dislocation creep leads to the decoupling of lithosphere from the asthenosphere via lubrication, and to reduced stress acting on the lithosphere although local convective vigor increases (Tackley, 2000b). This decou-

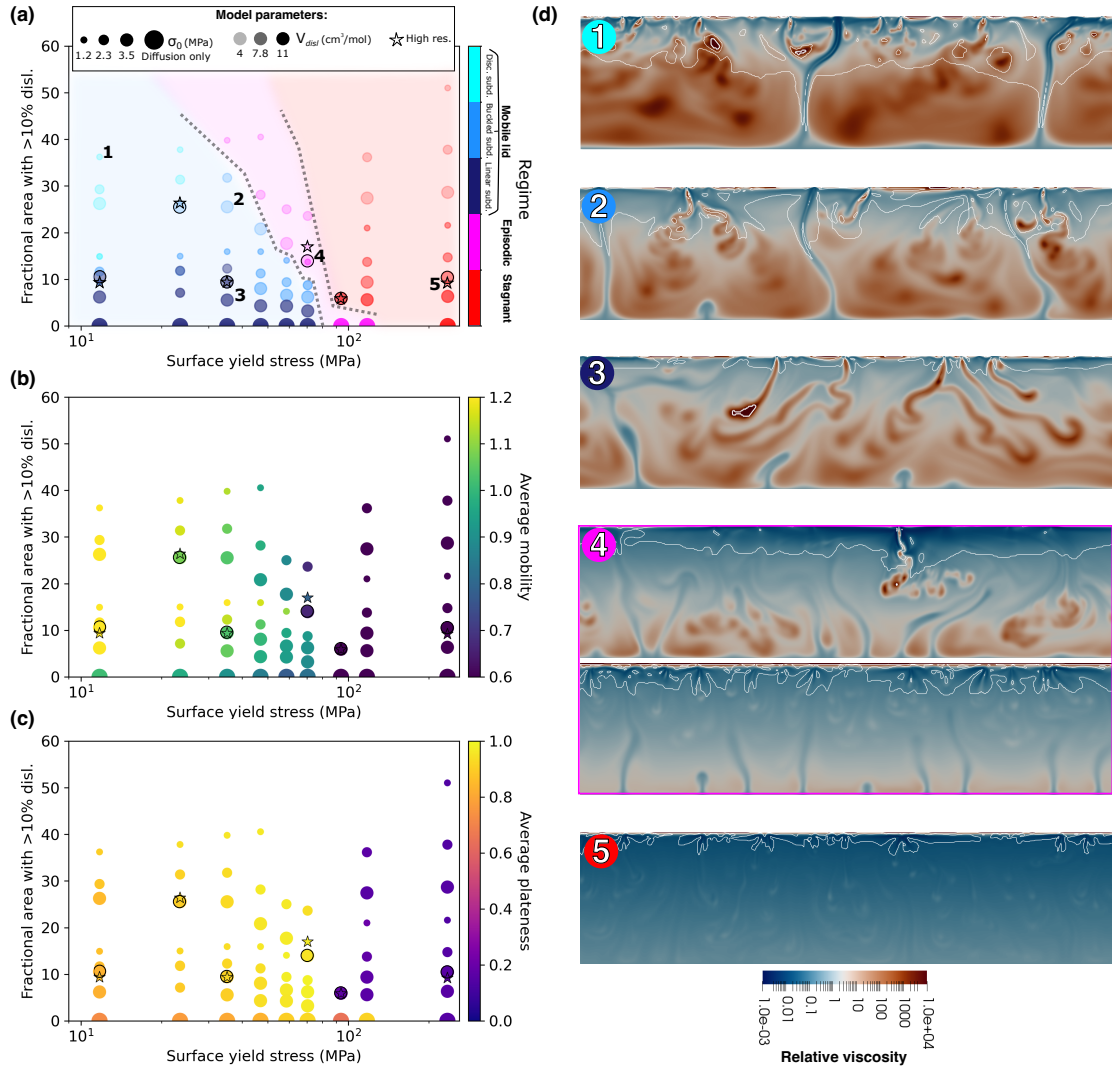


Figure 4. (a) Regime diagram of all models. Mobile-lid models have discontinuous and short-lived subductions (cyan), buckled slabs (blue), or mostly linear slabs (deep-blue). Episodic models (magenta) have intermediate plateness and mobility. Stagnant-lid models (red) have low plateness and mobility. Qualitative boundaries are drawn between each regime. (b-c) Similar to (a) but with colours representing time-averaged surface mobility and plateness, respectively. (d) Snapshots of viscosity of selected models referred as numbers in (a). White lines contour low-viscosity regions with >10% dislocation creep.

234 pling contributes to the observed increase in mobility. Since dislocation creep also fa-
 235vors lithosphere thinning, the plastic strength at lithospheric base is reduced compared
 236to models in pure diffusion creep. Therefore, an increasing amount of dislocation creep

237 enhances thin slab break-offs. Accounting for composite rheology in models with a low
 238 lithospheric strength thus enhances mobile-lid convection.

239 **3.2.2 Models with a strong lithosphere (>35 MPa)**

240 Models in pure diffusion creep with surface yield stresses comprised between ~ 35 MPa
 241 and ~ 120 MPa are also still in the mobile-lid regime. Including composite rheology with
 242 decreasing values of V_{disl} and/or σ_0 results in up to 40 % of the mantle being affected
 243 by dislocation creep (Fig. 3b and 4a-c).

244 For small amounts of dislocation creep in the mantle ($<20\%$), both plateness and
 245 surface mobility tend to increase by a factor of up to 1.4 and the number of slabs remains
 246 stable (Fig. 3b). In these models, thin low-viscosity asthenospheric areas tend to lubri-
 247 cate the base of the lithosphere, enhancing plate mobility and plateness (e.g. Tackley,
 248 2000b).

249 When the proportion of dislocation creep exceeds 20%, the number of active sub-
 250 ductions, plateness, and surface mobility decrease (Fig. 3b, 4a-c, and S5b). Lithosphere-
 251 asthenosphere decoupling promotes episodic and stagnant-lid convection (Fig. 4). This
 252 strengthening phenomenon due to large viscosity contrasts between the convecting man-
 253 tle and the lithosphere has long been demonstrated using Newtonian rheology (e.g. Moresi
 254 & Solomatov, 1995; Solomatov, 1995; Höink et al., 2012, although the latter study in-
 255 voked a flow channelization effect as being responsible for stagnant-lid convection) and
 256 non-Newtonian rheology in the asthenosphere (Semple & Lenardic, 2020, although they
 257 did not employ temperature- and depth-dependent viscosity, in contrast to the present
 258 study).

259 We further tested higher surface yield stresses (>120 MPa), which led to contin-
 260 uous stagnant-lid behavior irrespective of our choice of activation parameters. Like in
 261 models with a lower yield stress, decreasing V_{disl} and/or σ_0 produces a thickening of the
 262 layer containing dislocation creep. Although the convective regime remains unchanged
 263 in these models, changing the amount of dislocation creep can strongly decrease the vis-
 264 cosity in the asthenosphere and decrease lithospheric thickness by up to 60%. These ef-
 265 fects could have a large impact on the distribution of partial melting and the rates of
 266 magmatism on stagnant-lid planets (e.g. Schulz et al., 2020; Tosi & Padovan, 2021). How-
 267 ever, these models also suggest that once a stagnant-lid is established with a pure dif-

268 fusion creep rheology, adding composite rheology in the upper-mantle does not promote
269 the generation of more plate-like behavior.

270 4 Discussion and conclusion

271 4.1 Model assumptions

272 Model setup simplifications potentially alter mantle flow and therefore the spatio-
273 temporal diffusion/dislocation creep partitioning. Our models are limited to 2D-cartesian,
274 have a reference Rayleigh number ~ 10 times lower than Earth's, lower lithospheric strengths
275 than inferred from laboratory experiments (e.g. Brace & Kohlstedt, 1980), and lower ac-
276 tivation parameters for olivine than those predicted by rock experiments (e.g. Hirth &
277 Kohlstedt, 2003). We do not consider multiple mantle and lithosphere compositions and
278 phases (e.g. King, 2016). We also only tested one initial thermal state for our models
279 with composite rheology although different initial conditions could lead to distinct regime
280 boundaries for diffusion-creep-only and composite rheology, as shown in e.g. Semple and
281 Lenardic (2021); Weller and Lenardic (2018).

282 However, our mobile-lid models still produce mantle velocities of the order of the
283 cm/yr (Fig. 2a), oceanic lithosphere thickness of 100-200 km, and successfully generate
284 dislocation creep where it is expected to occur from rock-deformation experiments (Fig.
285 1). We also note no significant difference when increasing the resolution (Fig. 4a-c, star
286 symbols). Therefore, we anticipate that the general convective and tectonic trends (Fig.
287 4) and physical mechanisms described in this study still apply using more Earth-like se-
288 tups. In particular, we obtain a self-generated and self-evolving low-viscosity astheno-
289 sphere without invoking water and/or partial melting (King, 2016; Semple & Lenardic,
290 2020), the latter being often called on to justify the use of weakening laws to improve
291 plateness in whole-mantle Newtonian models (e.g. Tackley, 2000a; Bello et al., 2015).

292 Importantly, we assumed a uniform static grain-size, although rock-deformation
293 experiments indicate that diffusion creep should strongly depend on grain-size evolution
294 (Eq. 1). In some stagnant-lid models, we increased the static grain size, which produced
295 an increase in mantle average viscosity, stress, and proportion of dislocation creep in the
296 uppermost mantle (Fig. S6), associated with lithospheric thickening, as already described
297 in Schulz et al. (2020). This test, applied to models without dynamic grain-growth and
298 reduction, reveals the competing effects of large grain size (which tends to increase man-

299 tle viscosity) and large amounts of dislocation creep (which tend to decrease it) on litho-
300 sphere thickness, at least up to a doubling of static grain-size with our setup (Fig. S6).
301 Further exploring the role of grain-size evolution in mobile-lid scenarios is therefore needed
302 to further understand the role of composite rheology on mantle and lithosphere dynam-
303 ics.

304 **4.2 Earth’s observations and composite rheology in the uppermost man-** 305 **tle**

306 On Earth, seismic anisotropy, through the generation of dislocation creep-induced
307 LPO (e.g. Nicolas & Christensen, 1987), can provide complementary insight on the lat-
308 eral variations of mantle rheological properties (e.g. Becker et al., 2008). Although 3D
309 modeling is required to quantitatively compare the diffusion/dislocation creep partition-
310 ing in our models with observed seismic anisotropy, our results already potentially ex-
311 plain its observed orientation and strength variations (e.g. Debayle et al., 2005), as well
312 as high strength around slabs (e.g. Jadamec & Billen, 2012) and in the thermal trail of
313 plumes (e.g. Barruol et al., 2019). The correlation between strong anisotropy and fast
314 plate velocities described in Debayle and Ricard (2013) could also partly result from the
315 fact that these plates are attached to fast sinking slabs, thus favoring more dislocation
316 creep due to lithosphere basal shear. One future direction would therefore be to estimate
317 seismic anisotropy in more Earth-like models with composite rheology and compare it
318 to Earth’s observations (e.g. Kendall et al., 2022). Together with the consideration that
319 some rheological parameters are inter-dependent (e.g. Jain et al., 2019), this should pro-
320 vide complementary constraints on the range of rheological parameters applicable to Earth.
321 Finally, another independent constraint could come from the study of how composite rhe-
322 ology affects the spatio-temporal distribution of surface dynamic topography, both on
323 the long-term (e.g. Bodur & Rey, 2019) and on shorter glacial-isostatic-adjustment timescales
324 (Kang et al., 2022).

325 In this study, we show that our choice of composite rheological parameters impacts
326 uppermost mantle spatio-temporal viscosity variations and dynamics, therefore affect-
327 ing convection and surface tectonics in a non-linear way: at low lithospheric strength,
328 increasing the proportion of mantle deforming through dislocation creep promotes plate
329 mobility as well as numerous, weaker and short-lived slabs. In contrast, increasing the
330 proportion of mantle containing dislocation creep in models with large lithospheric strength,

331 results in episodic to stagnant-lid convection. This shows the potential geodynamical in-
332 fluence of experimental uncertainties of the rheological parameters and calls for both fur-
333 ther experimental refinement of mantle rheological parameters such as V_{disl} , and further
334 exploration of the effects of composite rheology on mantle convective planform and sur-
335 face tectonics in more sophisticated planetary-scale models.

336 Open Research

337 The convection code StagYY (Tackley, 2008) is property of ETH Zurich and Paul
338 J. Tackley. Data files used in this study can be downloaded from Arnould (2022).

339 Acknowledgments

340 This research benefited from Norwegian Research Council funding to the Centre for Earth
341 Evolution and Dynamics (223272) and to TR (PLATONICS, 276032). MA benefited from
342 INSU-PNP and UCBL-BQR fundings. Computations were performed on Stallo and Saga
343 Uninett Sigma2 facilities (nn9010k, ns9010k). Crameri et al. (2020) authored Fig.4d col-
344 ormap.

345 References

- 346 Alisic, L., Gurnis, M., Stadler, G., Burstedde, C., & Ghattas, O. (2012). Multi-
347 scale dynamics and rheology of mantle flow with plates. *Journal of Geophys-*
348 *ical Research: Solid Earth*, *117*(B10), 148–227. doi: [https://doi.org/10.1029/](https://doi.org/10.1029/2012JB009234)
349 [2012JB009234](https://doi.org/10.1029/2012JB009234)
- 350 Allmann, B. P., & Shearer, P. M. (2009). Global variations of stress drop for mod-
351 erate to large earthquakes. *Journal of Geophysical Research: Solid Earth*,
352 *114*(B1).
- 353 Arnould, M. (2022, Apr). *Effects of composite rheology on plate-like behaviour in*
354 *global-scale mantle convection [dataset]*. OSF. Retrieved from osf.io/p3mvm
- 355 Arnould, M., Coltice, N., Flament, N., Seigneur, V., & Muller, R. D. (2018). On the
356 scales of dynamic topography in whole-mantle convection models. *Geochem-*
357 *istry, Geophysics, Geosystems*, *19*(9), 3140–3163.
- 358 Asaadi, N., Ribe, N. M., & Sobouti, F. (2011). Inferring nonlinear mantle rheology
359 from the shape of the hawaiian swell. *Nature*, *473*(7348), 501–504.
- 360 Barruol, G., Sigloch, K., Scholz, J.-R., Mazzullo, A., Stutzmann, E., Montagner,

- 361 J.-P., ... others (2019). Large-scale flow of indian ocean asthenosphere driven
362 by réunion plume. *Nature Geoscience*, *12*(12), 1043–1049.
- 363 Becker, T. W., Chevrot, S., Schulte-Pelkum, V., & Blackman, D. K. (2006). Statis-
364 tical properties of seismic anisotropy predicted by upper mantle geodynamic
365 models. *Journal of Geophysical Research: Solid Earth*, *111*(B8).
- 366 Becker, T. W., Kustowski, B., & Ekström, G. (2008). Radial seismic anisotropy as
367 a constraint for upper mantle rheology. *Earth and Planetary Science Letters*,
368 *267*(1-2), 213–227.
- 369 Beghein, C., Yuan, K., Schmerr, N., & Xing, Z. (2014). Changes in seismic
370 anisotropy shed light on the nature of the gutenber g discontinuity. *Science*,
371 *343*(6176), 1237–1240.
- 372 Bello, L., Coltice, N., Tackley, P. J., Müller, R. D., & Cannon, J. (2015). Assessing
373 the role of slab rheology in coupled plate-mantle convection models. *Earth and*
374 *Planetary Science Letters*, *430*, 191–201.
- 375 Billen, M. I., & Hirth, G. (2005). Newtonian versus non-newtonian upper mantle
376 viscosity: Implications for subduction initiation. *Geophysical Research Letters*,
377 *32*(19). doi: <https://doi.org/10.1029/2005GL023457>
- 378 Billen, M. I., & Hirth, G. (2007). Rheologic controls on slab dynamics. *Geo-*
379 *chemistry, Geophysics, Geosystems*, *8*(8). doi: [https://doi.org/10.1029/](https://doi.org/10.1029/2007GC001597)
380 [2007GC001597](https://doi.org/10.1029/2007GC001597)
- 381 Bodur, Ö. F., & Rey, P. F. (2019). The impact of rheological uncertainty on dy-
382 namic topography predictions. *Solid Earth*, *10*(6), 2167–2167.
- 383 Brace, W. F., & Kohlstedt, D. L. (1980). Limits on lithospheric stress imposed
384 by laboratory experiments. *Journal of Geophysical Research: Solid Earth*,
385 *85*(B11), 6248–6252. Retrieved from [https://agupubs.onlinelibrary.wiley](https://agupubs.onlinelibrary.wiley.com/doi/abs/10.1029/JB085iB11p06248)
386 [.com/doi/abs/10.1029/JB085iB11p06248](https://agupubs.onlinelibrary.wiley.com/doi/abs/10.1029/JB085iB11p06248) doi: [https://doi.org/10.1029/](https://doi.org/10.1029/JB085iB11p06248)
387 [JB085iB11p06248](https://doi.org/10.1029/JB085iB11p06248)
- 388 Christensen, U. (1983). Convection in a variable-viscosity fluid: Newtonian versus
389 power-law rheology. *Earth and Planetary Science Letters*, *64*(1), 153–162.
- 390 Christensen, U. (1984). Convection with pressure-and temperature-dependent non-
391 newtonian rheology. *Geophysical Journal International*, *77*(2), 343–384.
- 392 Coltice, N., Gérard, M., & Ulvrová, M. (2017). A mantle convection perspective on
393 global tectonics. *Earth-science reviews*, *165*, 120–150.

- 394 Cramer, F., Shephard, G. E., & Heron, P. J. (2020). The misuse of colour in science
395 communication. *Nature communications*, *11*(1), 1–10.
- 396 Dannberg, J., Eilon, Z., Faul, U., Gassmüller, R., Moulik, P., & Myhill, R. (2017).
397 The importance of grain size to mantle dynamics and seismological observa-
398 tions. *Geochemistry, Geophysics, Geosystems*, *18*(8), 3034–3061.
- 399 Debayle, E., Kennett, B., & Priestley, K. (2005). Global azimuthal seismic
400 anisotropy and the unique plate-motion deformation of australia. *Nature*,
401 *433*(7025), 509–512.
- 402 Debayle, E., & Ricard, Y. (2013). Seismic observations of large-scale deformation
403 at the bottom of fast-moving plates. *Earth and Planetary Science Letters*, *376*,
404 165–177.
- 405 Garel, F., Thoraval, C., Tommasi, A., Demouchy, S., & Davies, D. R. (2020).
406 Using thermo-mechanical models of subduction to constrain effective man-
407 tle viscosity. *Earth and Planetary Science Letters*, *539*, 116243. doi:
408 <https://doi.org/10.1016/j.epsl.2020.116243>
- 409 Hall, C. E., & Parmentier, E. (2003). Influence of grain size evolution on convective
410 instability. *Geochemistry, Geophysics, Geosystems*, *4*(3). doi: [https://doi.org/](https://doi.org/10.1029/2002GC000308)
411 [10.1029/2002GC000308](https://doi.org/10.1029/2002GC000308)
- 412 Hedjazian, N., Garel, F., Davies, D. R., & Kaminski, E. (2017). Age-independent
413 seismic anisotropy under oceanic plates explained by strain history in the
414 asthenosphere. *Earth and Planetary Science Letters*, *460*, 135–142.
- 415 Hirth, G., & Kohlstedt, D. (2003). Rheology of the upper mantle and the man-
416 tle wedge: A view from the experimentalists. *Geophysical Monograph-American*
417 *Geophysical Union*, *138*, 83–106.
- 418 Höink, T., Lenardic, A., & Richards, M. (2012). Depth-dependent viscosity and
419 mantle stress amplification: implications for the role of the asthenosphere in
420 maintaining plate tectonics. *Geophysical Journal International*, *191*(1), 30–41.
- 421 Holt, A. F., & Becker, T. W. (2016). The effect of a power-law mantle viscosity on
422 trench retreat rate. *Geophysical Journal International*, 491–507.
- 423 Jadamec, M., & Billen, M. (2010). Reconciling surface plate motions with rapid
424 three-dimensional mantle flow around a slab edge. *Nature*, *465*(7296), 338–
425 341.
- 426 Jadamec, M., & Billen, M. I. (2012). The role of rheology and slab shape

- 427 on rapid mantle flow: Three-dimensional numerical models of the alaska
428 slab edge. *Journal of Geophysical Research: Solid Earth*, 117(B2). doi:
429 <https://doi.org/10.1029/2011JB008563>
- 430 Jain, C., Korenaga, J., & Karato, S.-i. (2018). On the grain size sensitivity of olivine
431 rheology. *Journal of Geophysical Research: Solid Earth*, 123(1), 674–688.
- 432 Jain, C., Korenaga, J., & Karato, S.-i. (2019). Global analysis of experimental data
433 on the rheology of olivine aggregates. *Journal of Geophysical Research: Solid
434 Earth*, 124(1), 310–334.
- 435 Kang, K., Zhong, S., Geruo, A., & Mao, W. (2022). The effects of non-newtonian
436 rheology in the upper mantle on relative sea level change and geodetic observ-
437 ables induced by glacial isostatic adjustment process. *Geophysical Journal
438 International*, 228(3), 1887–1906.
- 439 Karato, S.-i., & Wu, P. (1993). Rheology of the upper mantle: A synthesis. *Science*,
440 260(5109), 771–778.
- 441 Kendall, E., Faccenda, M., Ferreira, A., & Chang, S.-J. (2022). On the relationship
442 between oceanic plate speed, tectonic stress, and seismic anisotropy. *Geophysi-
443 cal Research Letters*, 49(15), e2022GL097795.
- 444 King, S. D. (2016). An evolving view of transition zone and midmantle viscosity.
445 *Geochemistry, Geophysics, Geosystems*, 17(3), 1234–1237.
- 446 Korenaga, J., & Karato, S.-I. (2008). A new analysis of experimental data on olivine
447 rheology. *Journal of Geophysical Research: Solid Earth*, 113(B2).
- 448 Li, M., & Zhong, S. (2019). Lateral motion of mantle plumes in 3-d geodynamic
449 models. *Geophysical Research Letters*, 46(9), 4685–4693.
- 450 Moresi, L.-N., & Solomatov, V. (1995). Numerical investigation of 2d convection
451 with extremely large viscosity variations. *Physics of Fluids*, 7(9), 2154–2162.
- 452 Neuharth, D., & Mittelstaedt, E. (2023). Temporal variations in plume flux: char-
453 acterizing pulsations from tilted plume conduits in a rheologically complex
454 mantle. *Geophysical Journal International*, 233(1), 338–358.
- 455 Nicolas, A., & Christensen, N. I. (1987). Formation of anisotropy in upper mantle
456 peridotites-a review. *Composition, structure and dynamics of the lithosphere-
457 asthenosphere system*, 16, 111–123.
- 458 Phipps Morgan, J., Morgan, W. J., Zhang, Y.-S., & Smith, W. H. (1995). Ob-
459 servational hints for a plume-fed, suboceanic asthenosphere and its role in

- 460 mantle convection. *Journal of Geophysical Research: Solid Earth*, 100(B7),
461 12753–12767.
- 462 Ranalli, G. (2001). Mantle rheology: radial and lateral viscosity variations inferred
463 from microphysical creep laws. *Journal of Geodynamics*, 32(4-5), 425–444.
- 464 Rolf, T., Capitanio, F. A., & Tackley, P. J. (2018). Constraints on mantle viscos-
465 ity structure from continental drift histories in spherical mantle convection
466 models. *Tectonophysics*, 746, 339–351.
- 467 Rozel, A. (2012). Impact of grain size on the convection of terrestrial planets. *Geo-*
468 *chemistry, Geophysics, Geosystems*, 13(10). doi: [https://doi.org/10.1029/](https://doi.org/10.1029/2012GC004282)
469 2012GC004282
- 470 Schulz, F., Tosi, N., Plesa, A.-C., & Breuer, D. (2020). Stagnant-lid convection with
471 diffusion and dislocation creep rheology: Influence of a non-evolving grain size.
472 *Geophysical Journal International*, 220(1), 18–36.
- 473 Semple, A., & Lenardic, A. (2020). The robustness of pressure-driven astheno-
474 spheric flow in mantle convection models with plate-like behavior. *Geophysical*
475 *Research Letters*, 47(17), e2020GL089556.
- 476 Semple, A., & Lenardic, A. (2021). Feedbacks between a non-newtonian upper man-
477 tle, mantle viscosity structure and mantle dynamics. *Geophysical Journal In-*
478 *ternational*, 224(2), 961–972.
- 479 Solomatov, V. (1995). Scaling of temperature-and stress-dependent viscosity convec-
480 tion. *Physics of Fluids*, 7(2), 266–274.
- 481 Stein, C., Schmalzl, J., & Hansen, U. (2004). The effect of rheological parameters on
482 plate behaviour in a self-consistent model of mantle convection. *Physics of the*
483 *Earth and Planetary Interiors*, 142(3-4), 225–255.
- 484 Tackley, P. J. (2000a). Self-consistent generation of tectonic plates in time-
485 dependent, three-dimensional mantle convection simulations. *Geochemistry,*
486 *Geophysics, Geosystems*, 1(8). doi: <https://doi.org/10.1029/2000GC000036>
- 487 Tackley, P. J. (2000b). Self-consistent generation of tectonic plates in time-
488 dependent, three-dimensional mantle convection simulations 2. strain weak-
489 ening and asthenosphere. *Geochemistry, Geophysics, Geosystems*, 1(8). doi:
490 <https://doi.org/10.1029/2000GC000043>
- 491 Tackley, P. J. (2008). Modelling compressible mantle convection with large viscosity
492 contrasts in a three-dimensional spherical shell using the yin-yang grid. *Physics*

- 493 *of the Earth and Planetary Interiors*, 171(1-4), 7–18. doi: <https://doi.org/10>
494 .1016/j.pepi.2008.08.005
- 495 Tosi, N., & Padovan, S. (2021). Mercury, moon, mars. In *Mantle convection and sur-*
496 *face expressions* (p. 455-489). American Geophysical Union (AGU). Retrieved
497 from <https://agupubs.onlinelibrary.wiley.com/doi/abs/10.1002/>
498 9781119528609.ch17 doi: <https://doi.org/10.1002/9781119528609.ch17>
- 499 Trompert, R., & Hansen, U. (1998). Mantle convection simulations with rheologies
500 that generate plate-like behaviour. *Nature*, 395(6703), 686–689.
- 501 Weller, M. B., & Lenardic, A. (2018). On the evolution of terrestrial planets:
502 Bi-stability, stochastic effects, and the non-uniqueness of tectonic states. *Geo-*
503 *science Frontiers*, 9(1), 91–102.

Figure 1.

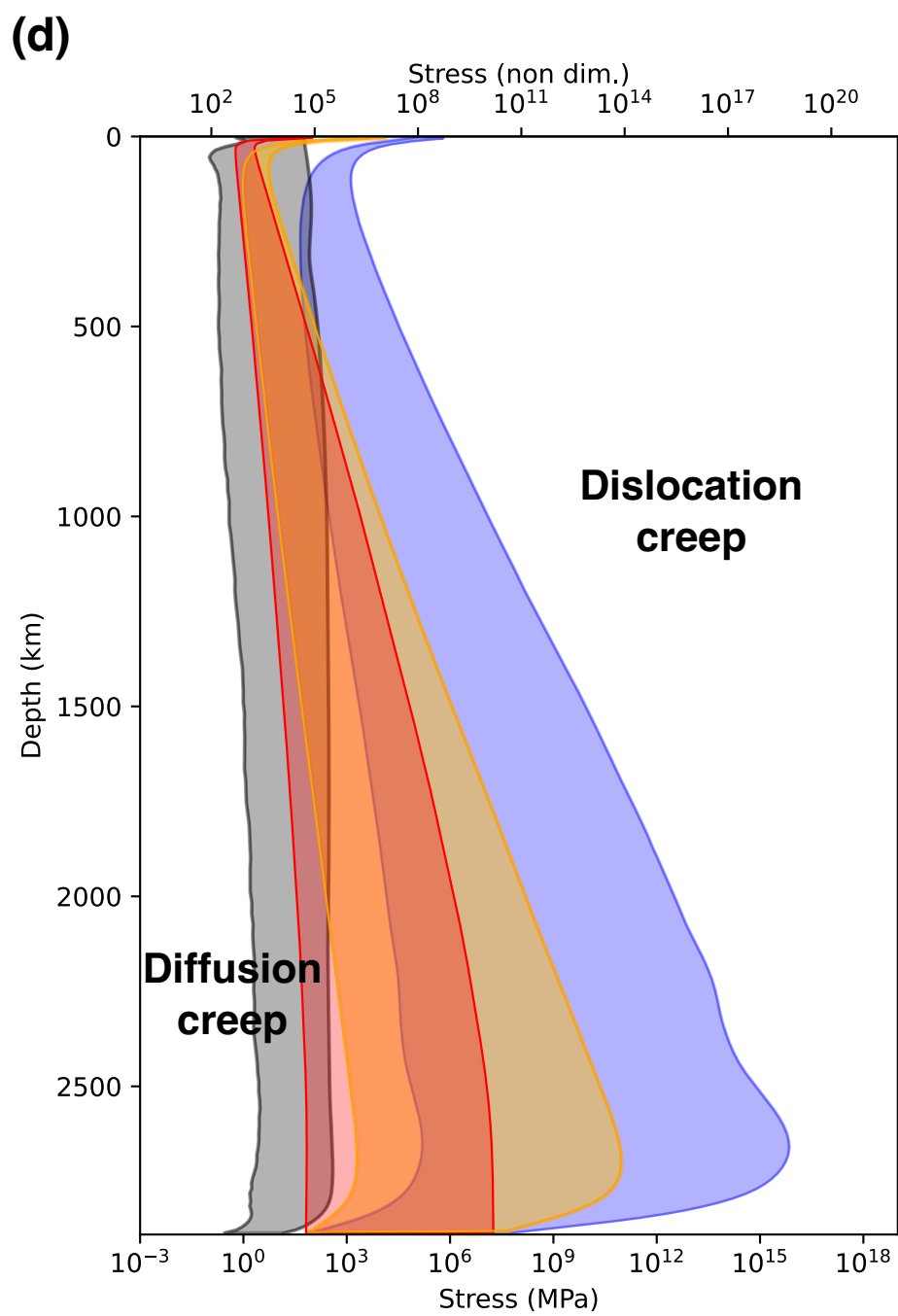
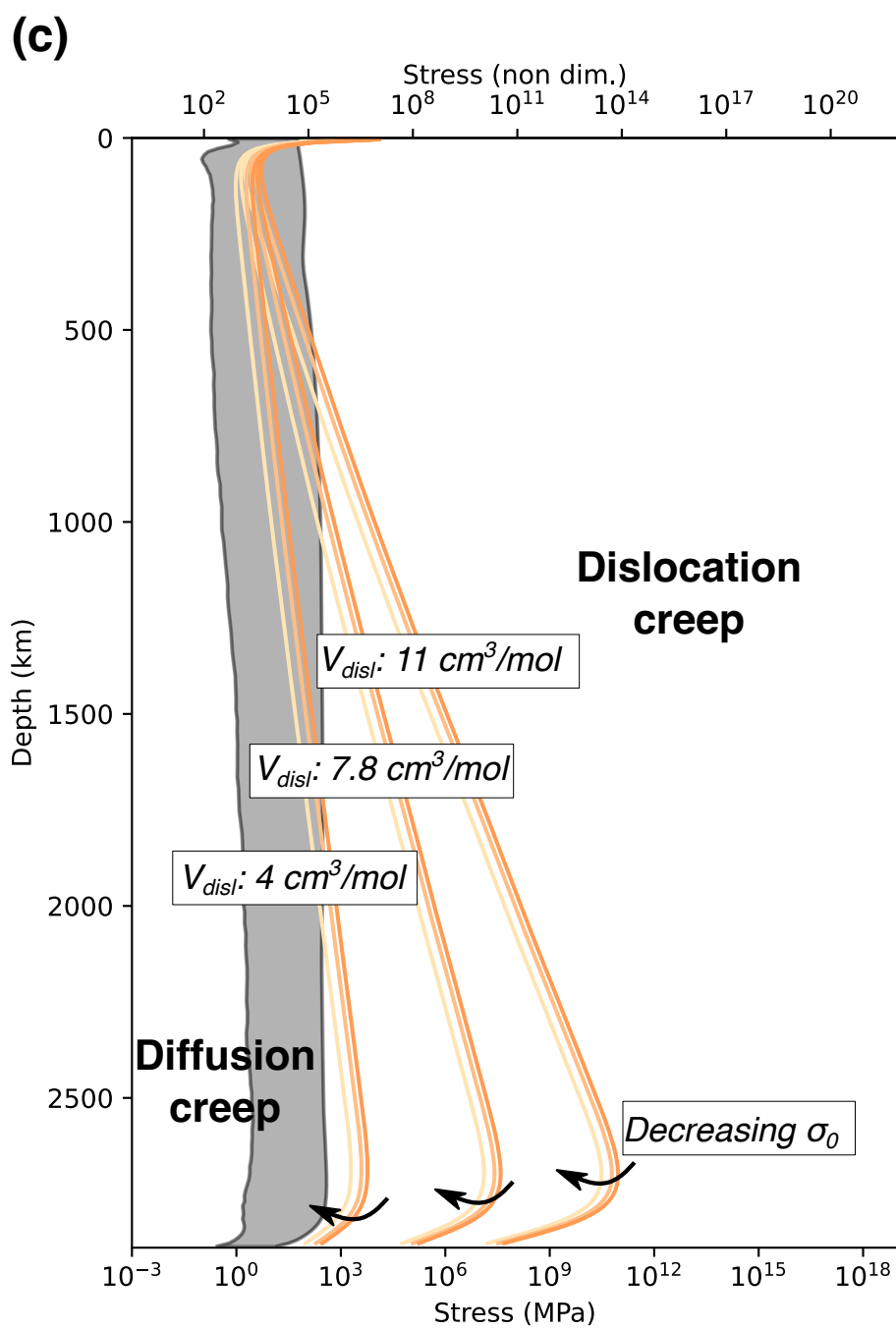
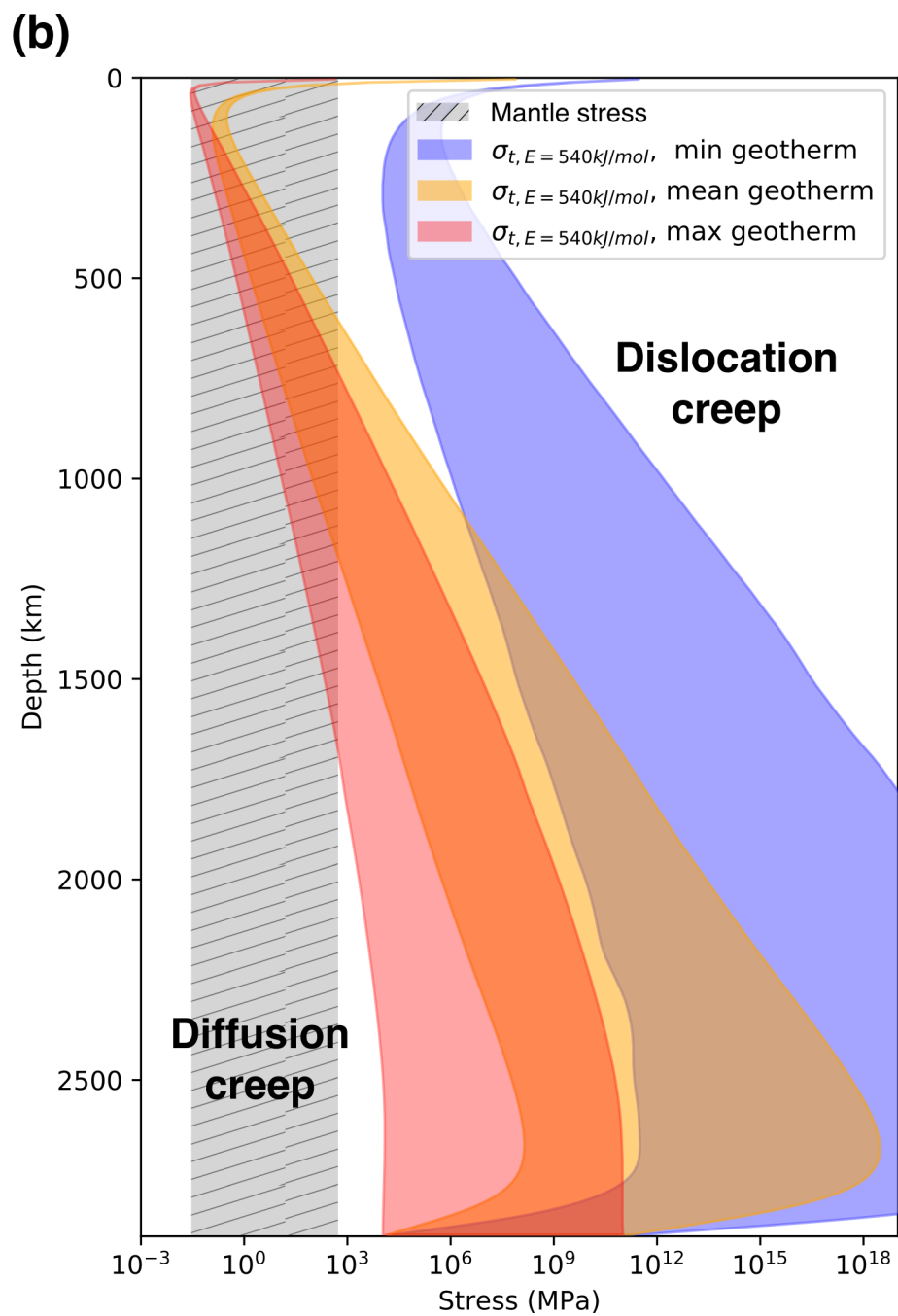
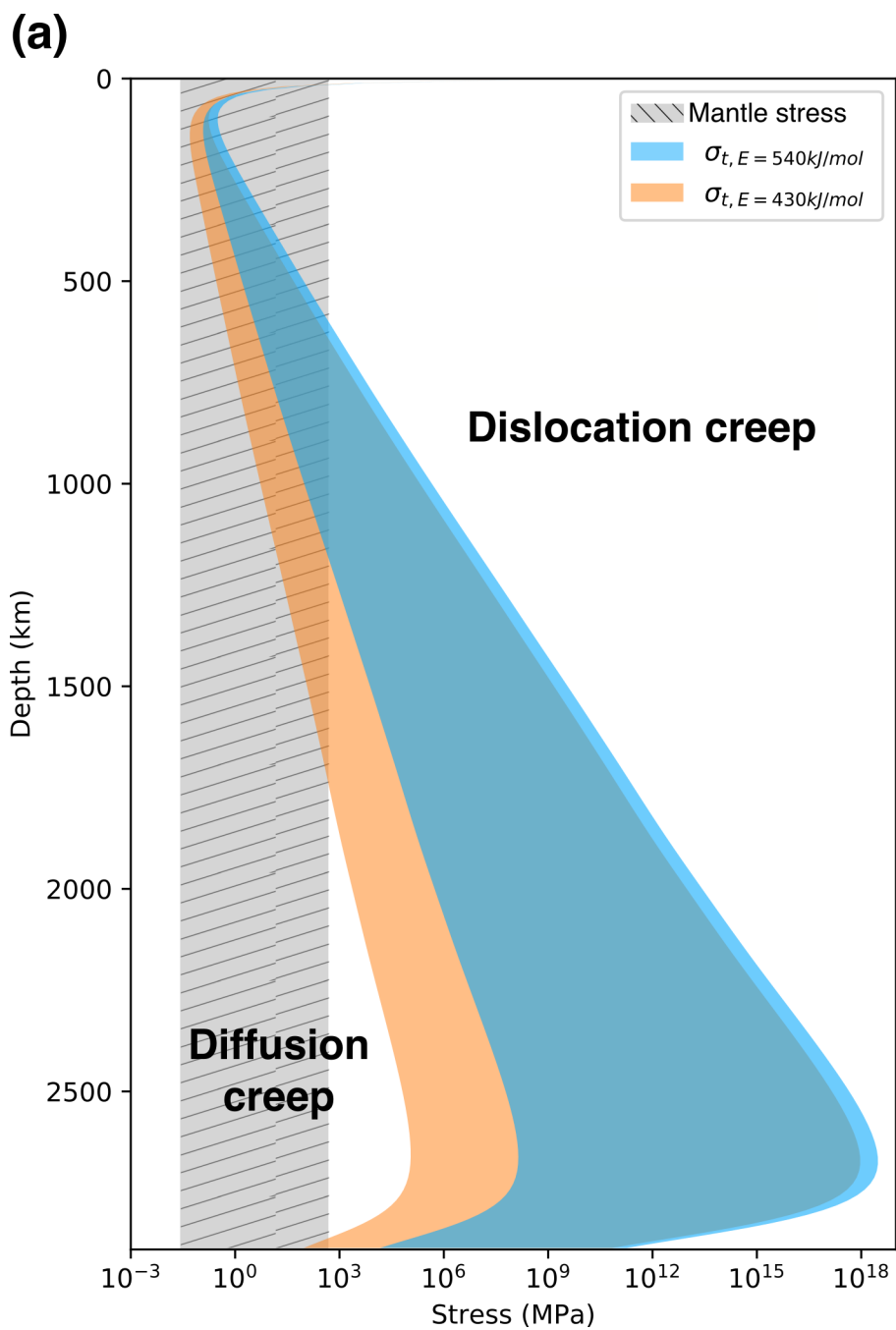


Figure 2.

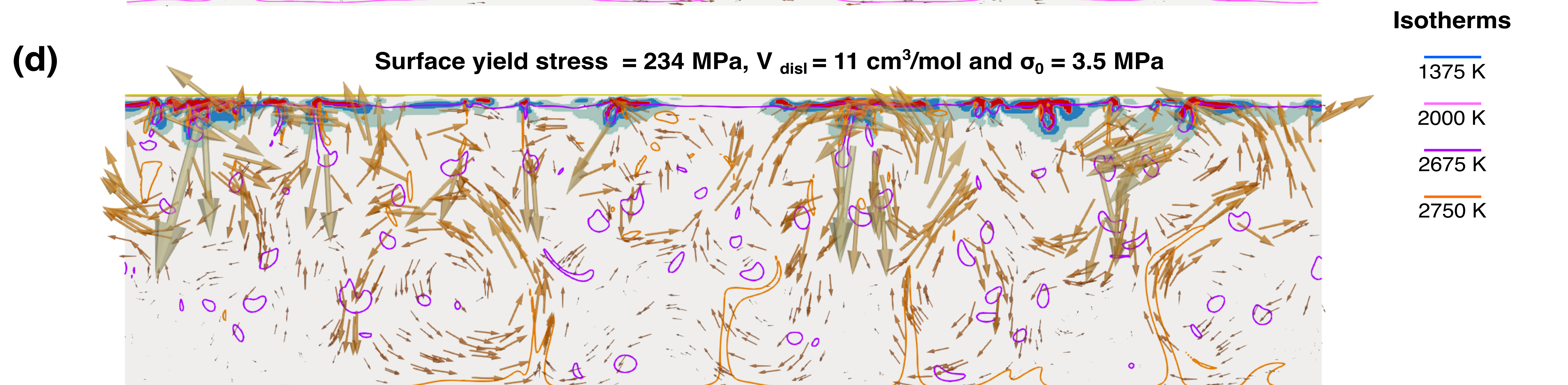
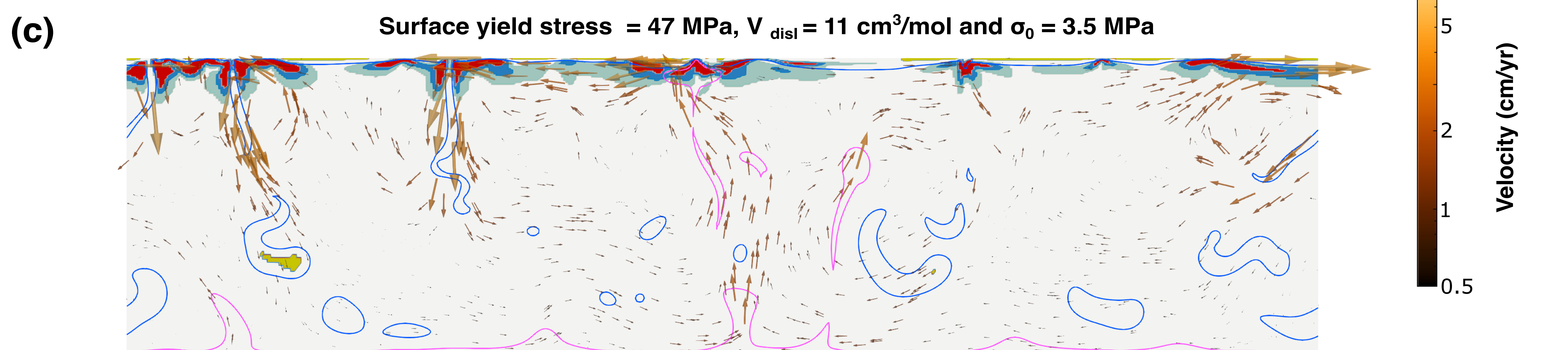
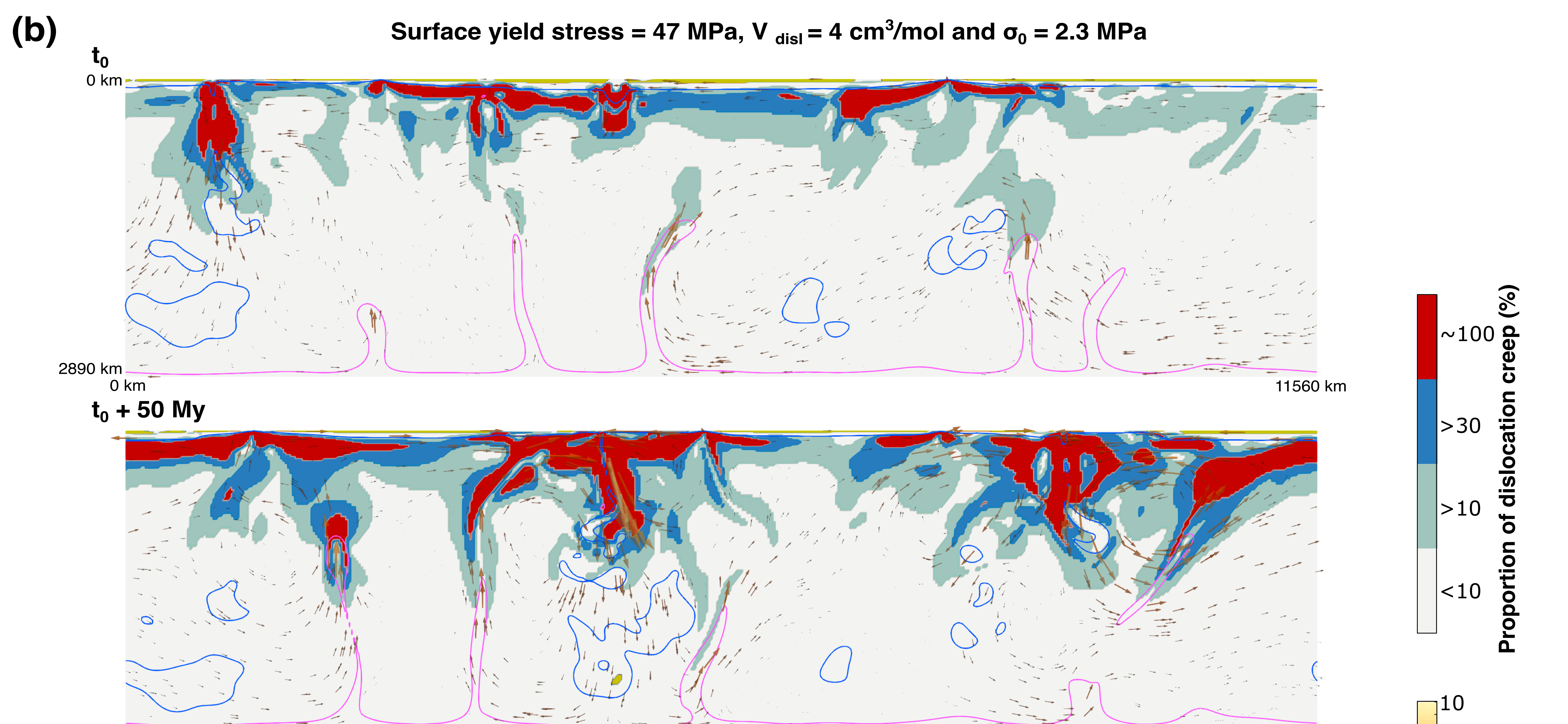
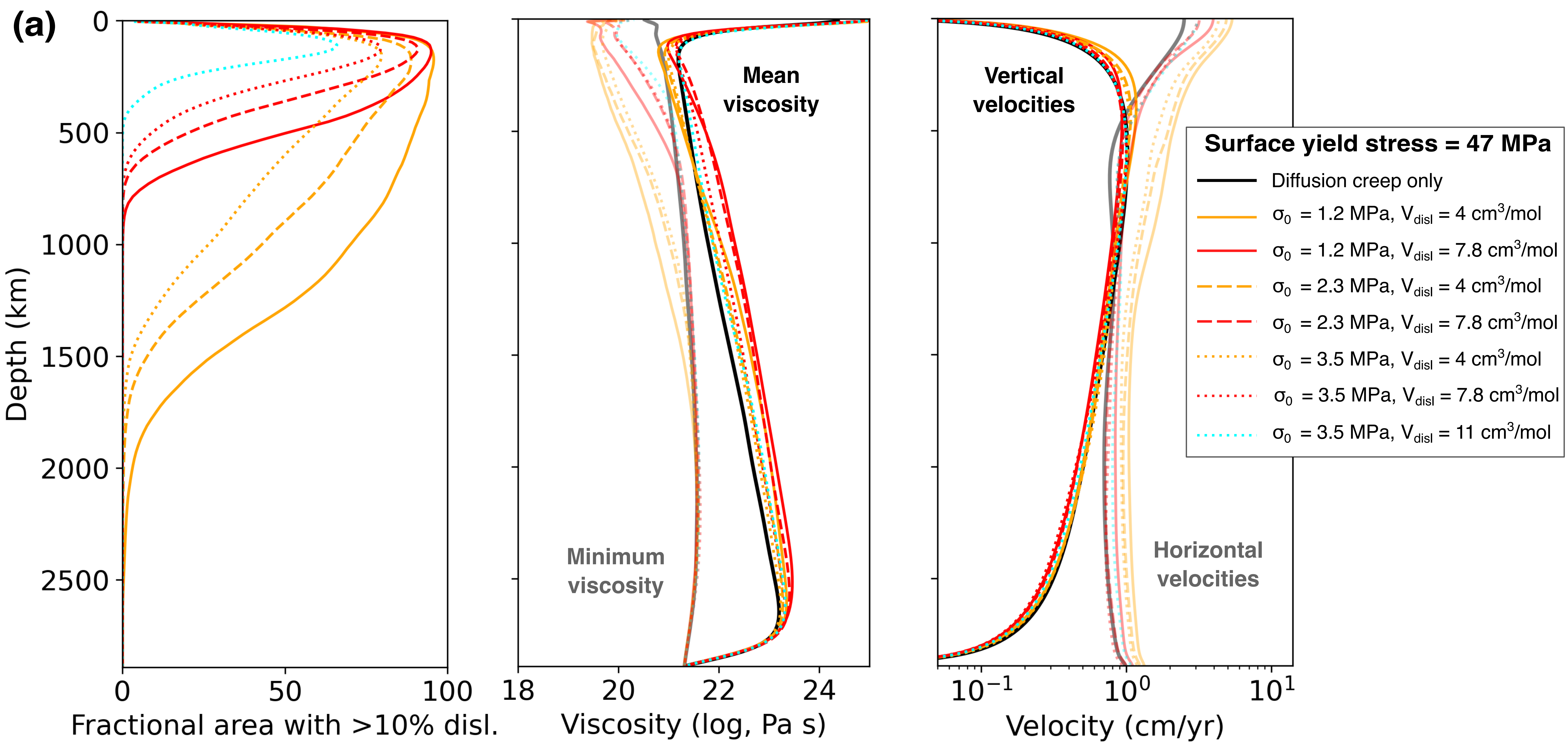


Figure 3.

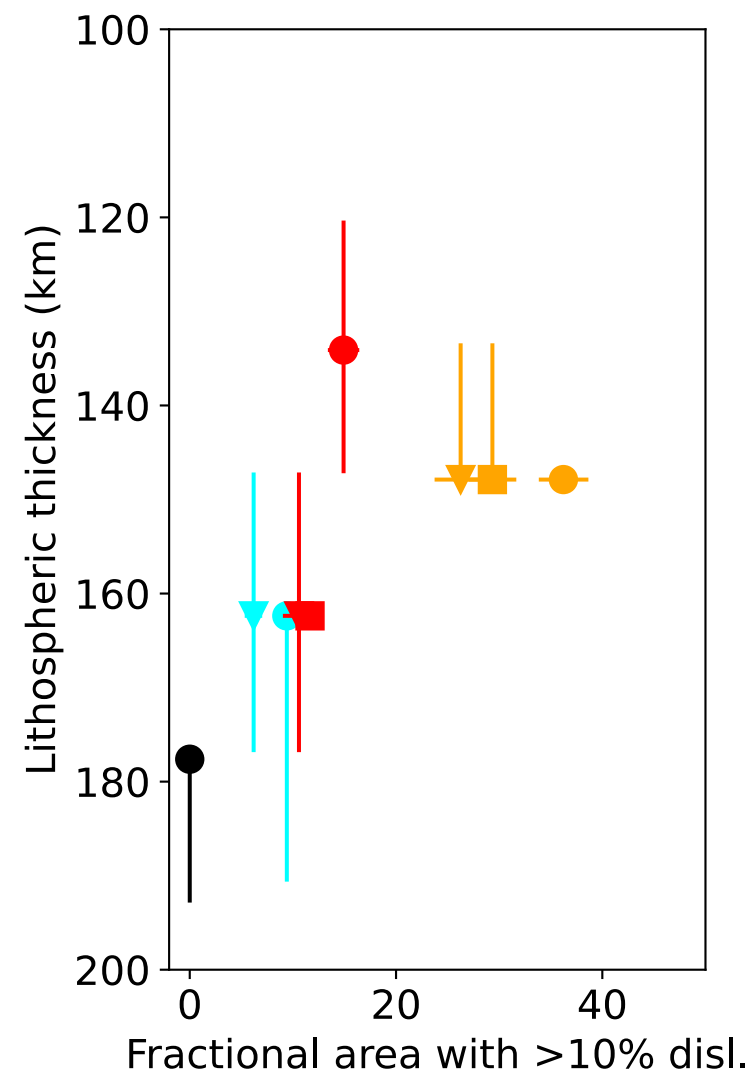
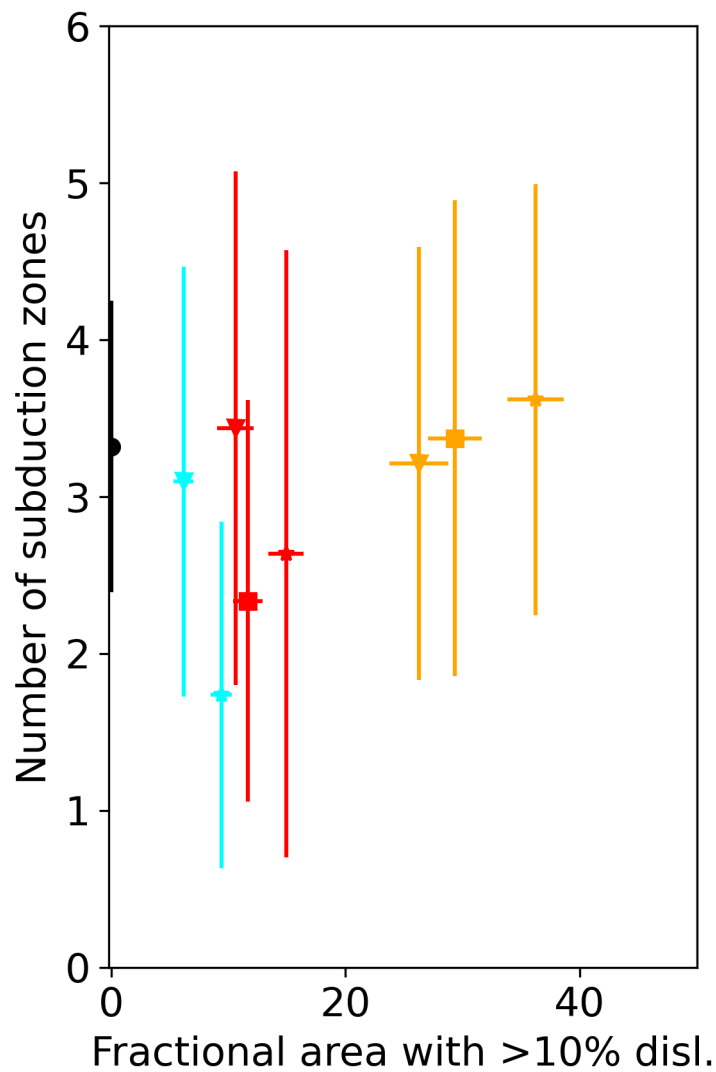
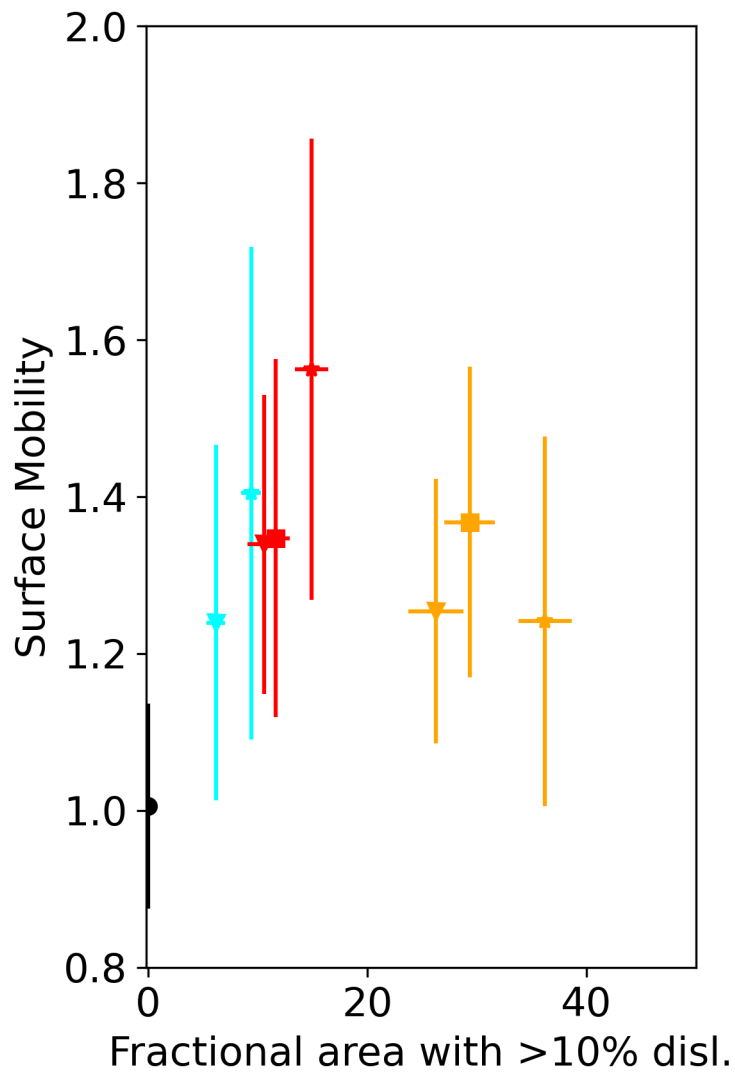
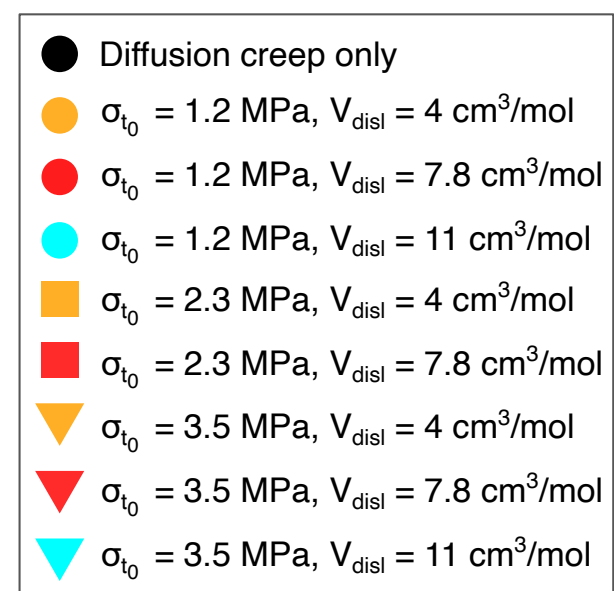
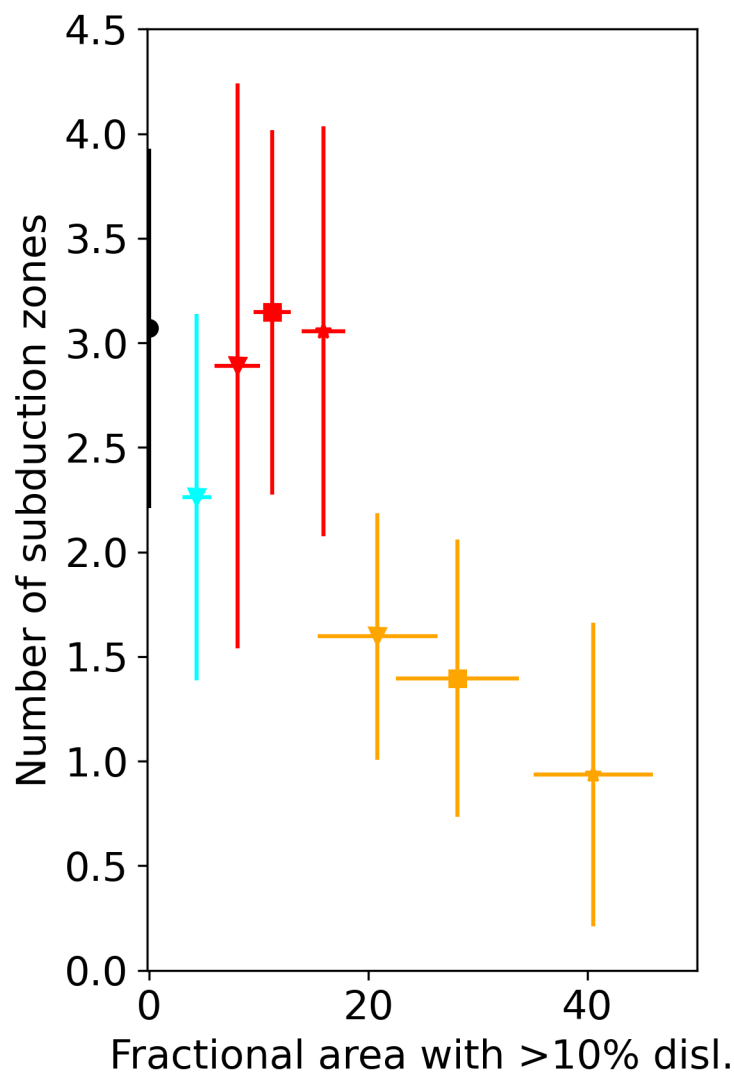
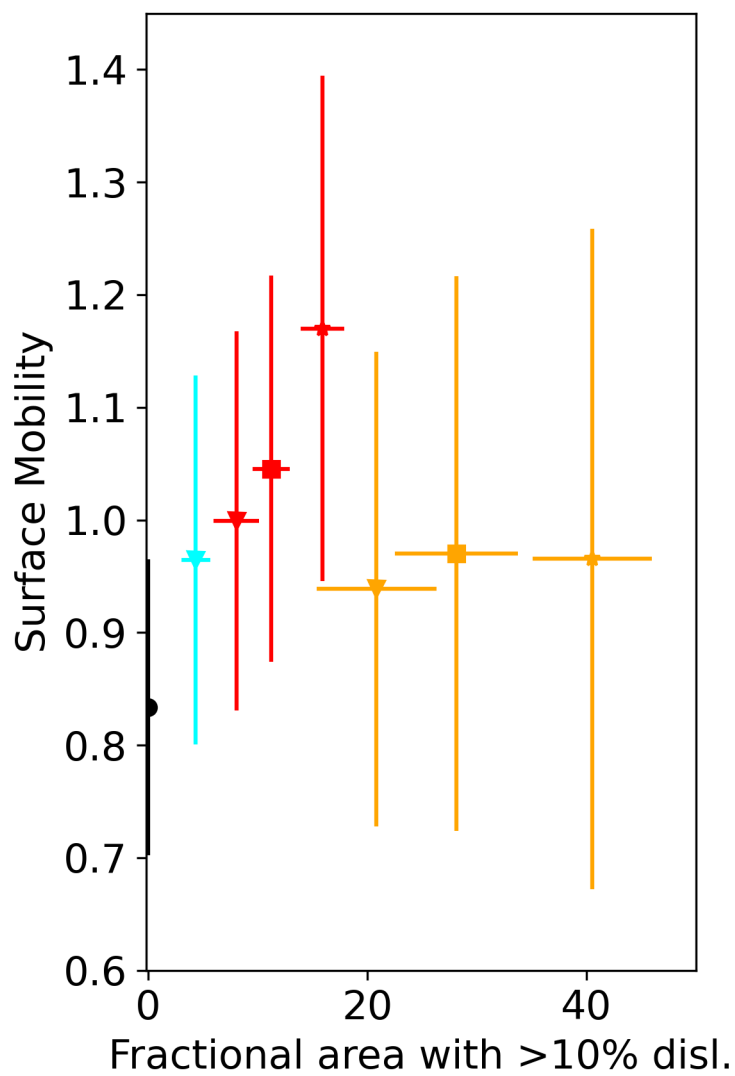
(a)**Surface yield stress: 12 MPa****(b)****Surface yield stress: 47 MPa**

Figure 4.

